

Mineralogical characterization and non-isothermal pyrolysis kinetics of Moroccan Rif oil shale

Ely Cheikh Moine¹ · Rajaa Bouamoud¹ · Adnane El Hamidi¹ · Mariam Khachani¹ · Mohammed Halim¹ · Said Arsalane¹

Received: 17 January 2017 / Accepted: 12 August 2017 / Published online: 30 August 2017
© Akadémiai Kiadó, Budapest, Hungary 2017

Abstract The mineralogical characterization and pyrolysis kinetics of raw oil shale from Moroccan Rif region and the corresponding bitumen-free material were investigated using various analytical techniques. The structural analysis results showed the siliceous character of mineral matrix and the presence of complex organic components in both oil shales studied. Non-isothermal pyrolysis kinetic measurements indicated that bitumen-free oil shale exhibits a single behavior pyrolysis in the oil-producing stage as compared to raw oil shale. The activation energies estimated by using isoconversional methods reveal that the pyrolysis reaction occurred by one-step kinetic process. The kinetic parameters, determined from a nonlinear fitting method using various kinetic models $g(\alpha)$ and iterative Kissinger–Akahira–Sunose energy calculations, reveal that the pyrolysis mechanism is well described by the n th order kinetics (Fn), with $n = 1.071$, for bitumen-free oil shale, and $n = 1.550$, for kerogen of raw oil shale. The mechanism of the whole pyrolysis process of raw oil shale seems not to be affected by the elimination of bitumen, but only some kinetic changes have been recorded in the reaction order mechanism. The process pyrolysis is represented by independent reactions and consequently considered as parallel processes. Besides, the thermodynamic functions of activated complexes (ΔS^\ddagger , ΔH^\ddagger and ΔG^\ddagger) were also calculated and the pyrolysis is found as non-spontaneous process in agreement with the thermal analysis data.

Keywords Mineralogical characterization · Oil shale · Kinetic analysis · Isoconversional methods · Activation energy

Introduction

Morocco is one of the few countries in the Mena region that lacks conventional fossil fuel resources such as oil or natural gas and depends heavily on foreign sources for over 97% of its energy supply. However, Morocco holds substantial oil shale reserves that can be economically converted into synthetic fuel and that make it a vital source of own economic development. According to the report published in 2013 by the World Council of Energy, Morocco ranks sixth worldwide in terms of oil shale reserves, way ahead of many countries in the Mena region such as Jordan and Turkey. Among the largest known Moroccan oil shale, one can cite Timahdit, Tarfaya and Tangier deposits which are located in central, southwestern and northern Morocco, respectively (Fig. 1). Several programs and developments on Moroccan oil shales have already been launched by many international oil companies, but to date, the commercial exploitation of oil has not yet been achieved.

Oil shale can be defined as an organic-rich sedimentary rock from which oil and/or gas can be produced by pyrolysis or by direct combustion as low-grade fuel for power generation and heating purposes [2]. Thus, it consists of solid organic matter entrained in a major amount of mineral matrix. The solid organic matter is classified into two components, natural bitumen, which constitutes the minor part, is soluble in conventional solvents, and an insoluble important fraction, called kerogen which consists of complex macromolecules with a kind of three-

✉ Said Arsalane
pr.saidarsalane@gmail.com

¹ Laboratory of Materials, Nanotechnology and Environment, Faculty of Sciences, University of Mohammed V, Avenue Ibn Battouta, BP: 1014, 10000 Rabat, Morocco

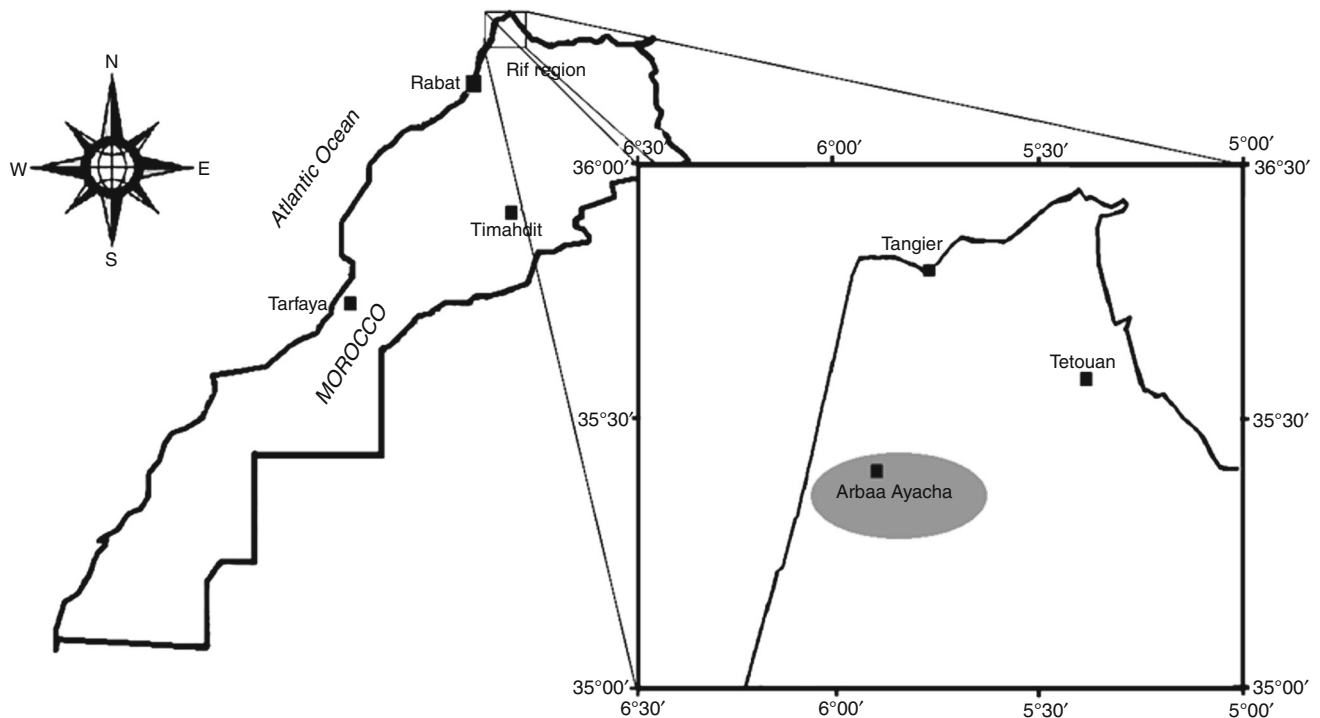


Fig. 1 Location of Moroccan Rif oil shale (Arbaa Ayacha deposit) [1]

dimensional structure that can yield a significant oil proportion of an appearance similar to some volatile light crude oils [3, 4]. The inorganic matrix consists mainly of quartz, clay, carbonates, pyrite and iron oxide besides traces of chemical elements such as Ni, Cu, Mo, Sr, Zn, Co and V [5, 6].

Thermogravimetric analysis (TG) has been extensively used as a means of investigating pyrolysis characteristics and kinetic parameters of processes, in particular to explore the effect of pyrolysis temperature and heating rate on oil shale decomposition [7–10]. The main region of mass loss corresponding to hydrocarbon oil and gas release was observed between 200 and 620 °C, in almost all the world's oil shale [11]. Mass loss details can be exploited to construct kinetic models using the isothermal and non-isothermal conditions of the thermal process. Many kinetic studies of oil shales have been carried out for several years, and they agreed that the pyrolysis reaction mechanism is complex and involves one or more processes [12–14]. However, some controversy has been raised in the kinetic results, notably on the estimation of the reaction mechanism and the models which give the best description of experimental data. Recently, a new approach to the non-isothermal kinetic of pyrolysis has been developed in order to separate the individual process observed in thermal behavior. It is based on the deconvolution procedure using different statistical functions, depending on the nature and shape of the kinetic curves. This approach has been well

documented for complex solid-state reactions by Perejón et al. [15] and Koga et al. [16]. For some oil shales, two main processes have been isolated from pyrolysis according to their origins and geological environments; the first one is assigned to the decomposition of bitumen while the other process is attributed to the degradation of kerogen into oil and gas. Both independent processes are mostly described by F_n -order reaction mechanism [17–19]. In this context and to better understand the effect of soluble organic matter on the thermal behavior of oil shales, it is convenient to separate the bitumen from the original rock and then to study only the kinetics of kerogen–oil shale. This procedure can simplify the thermal study and minimizes the complexity of processes involved during the pyrolysis.

The present research is an experimental study of oil shale from Arbaa Ayacha deposit, located in the Moroccan Rif region, by using a TG apparatus under non-isothermal conditions. The kinetic study was focused on crushed samples after removal of soluble bitumen. To our knowledge, few works have been devoted to shale rocks devoid of bitumen. The objective was to determine the kinetic triplet [activation energy E , exponential factor A and model function $g(\alpha)$] enabling to better describe the pyrolysis mechanism and to compare the present results with our recent research carried out on a crude sample of the analogous oil shale [1]. Kinetic modeling is also proposed and correlated with the experimental data.

Experimental

Materials

Oil shale rocks were collected from Arbaa Ayacha which is located in Rif region of northern Morocco (Fig. 1). A significant amount of shale was washed several times with distilled water to remove traces of soil and any impurities on the outer surface and then dried in air for 2 days and finally crushed intimately. To eliminate the soluble bitumen from shale rocks, a mass of about 100 g was treated with dichloromethane/methanol at proportion (2/1, v/v) using Soxhlet extraction apparatus and heated at temperature of 70 °C for 24 h. This operation was repeated twice to ensure the total elimination of the soluble bitumen. After centrifugation, the obtained residue was washed abundantly with hot water, dried in an oven at 60 °C for 48 h, and finally stored protected from humidity in a desiccator. The originate oil shale and bitumen-free oil shale from Arbaa Ayacha were named ROS and FOS, respectively. The kerogen-ROS means the peak in thermal curves corresponding to kerogen in originate oil shale, as has been shown in our previous study [1].

In our previous works, we have investigated the organic geochemical of raw oil shale from Arbaa Ayacha (ROS) [20, 21]. Herein, we present the Rock-Eval parameters results (Table 1).

Characterization methods

X-ray diffraction (XRD) is a non-destructive analysis technique generally used to identify the mineral phases present in oil shale. The XRD diagrams were collected using a Siemens D500 Powder Diffractometer equipped with copper anticathode ($\lambda_{\text{CuK}\alpha} = 1.541838 \text{ \AA}$) at scanning speed of $0.04 \text{ }^\circ\text{s}^{-1}$. X-ray fluorescence (XRF) analysis is used to quantify the elemental composition of inorganic materials. The analyses were carried out using PANalytical Epsilon 5 spectrometry system. Fourier transform infrared (FTIR) spectroscopy is used to obtain an infrared spectrum of absorption or emission of organic, polymeric and inorganic materials. The FTIR spectra were performed on a

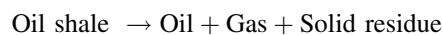
Table 1 Rock-Eval parameters of raw oil shale from Arbaa Ayacha (ROS) [20]

Total organic carbon (TOC, Mass%)	4.3
Volatile hydrocarbon (HC) content (S_1 , mg HC/g rock)	0.96
Remaining HC generative potential (S_2 , mg HC/g rock)	12.14
Hydrogen index (HI, mg HC/g TOC)	282
T_{max} , Temperature at maximum amount of organic S_2 hydrocarbons (°C)	440
Kerogen type II from marine origin	

Vertex 70 spectrometer equipped with a Digitec detector, via the conventional KBr pellet method. Samples were scanned in transmission mode with 4 cm^{-1} resolution, at the range of $4000\text{--}400 \text{ cm}^{-1}$. Thermal measurements were carried out to study the pyrolysis reaction of oil shale. The thermal curves were obtained on simultaneous thermogravimetry, derivative thermogravimetry and differential thermal analysis (TG/DTG/DTA) using LabsysTM Evo (1F) Setaram apparatus. To evaluate the kinetic parameters, the ICTAC (International Committee of Thermal Analysis and Calorimetry) kinetics committee recommendations for collecting experimental data and performing kinetics computations [22–24] were followed. Before analysis, the thermal analysis system was firstly calibrated for temperature reading with reference metals of 99.99% purity. It was also essential to calibrate the balance for buoyancy effects to allow quantitative estimation of mass changes. The experiments were conducted under non-isothermal conditions in pure nitrogen flow atmosphere of 60 mL min^{-1} from room temperature up to $1000 \text{ }^\circ\text{C}$, at various heating rates (5, 10, 15 and $20 \text{ }^\circ\text{C min}^{-1}$). The measurements were repeated three times in order to make certain the reproducibility and minimize the experimental errors. An initial mass of sample of $10.0 \pm 0.1 \text{ mg}$ was placed in an alumina pan. The sample was well dispersed with negligible depth to reduce heat and mass transfers.

Kinetic background

The oil shale pyrolysis is a complicated process with the coexistence of diversified reaction mechanisms. Generally, the non-isothermal decomposition of oil shale can be described by simplified reaction as follows:



According to non-isothermal kinetic theory of solid state, the kinetic pyrolysis of oil shale can be expressed by the Arrhenius equation:

$$\frac{d\alpha}{dT} = \frac{A}{\beta} \exp\left(\frac{-E_\alpha}{RT}\right) f(\alpha) \quad (1)$$

where α is the degree of conversion, β is the heating rate ($^\circ\text{C min}^{-1}$), E_α is the apparent activation energy, A is the pre-exponential factor, R is the gas constant ($R = 8.314 \text{ J mol}^{-1} \text{ K}^{-1}$) and $f(\alpha)$ is the reaction model function that gives the information about the mechanism, as listed in Table 2. The kinetic parameters (E_α , A , $f(\alpha)$ or $g(\alpha)$), often called the kinetic triplet, can be determined from Eq. (1) by using several approaches, categorized generally into two method groups: model-fitting and model-free methods.

Table 2 Some basic mathematical models of the thermal kinetics in solid-state reactions

Reaction models	Symbol	$f(\alpha)$	$g(\alpha)$
1. Chemical process or mechanism non-invoking equations			
First-order	F1	$(1 - \alpha)^1$	$-\ln(1 - \alpha)$
Second-order	F2	$(1 - \alpha)^2$	$(1 - \alpha)^{-1} - 1$
Three-halves order kinetics	F3/2	$(1 - \alpha)^{3/2}$	$2[(1 - \alpha)^{-1/2} - 1]$
Third-order	F3	$(1 - \alpha)^3$	$[(1 - \alpha)^{-2} - 1]/2$
n th order kinetics ($n \neq 1$)	F n	$(1 - \alpha)^n$	$[1 - (1 - \alpha)^{1-n}]/(1 - n)$
2. Acceleratory rate equations			
Power law	P2	$2\alpha^{1/2}$	$\alpha^{1/2}$
Power law	P3	$3\alpha^{2/3}$	$\alpha^{1/3}$
Power law	P4	$4\alpha^{3/4}$	$\alpha^{1/4}$
3. Deceleratory rate Eqs. 3.1. Phase boundary reaction			
Contracting area	R2	$2(1 - \alpha)^{1/2}$	$1 - (1 - \alpha)^{1/2}$
Contracting volume	R3	$3(1 - \alpha)^{2/3}$	$1 - (1 - \alpha)^{1/3}$
3.2. Based on the diffusion mechanism			
One-dimensional diffusion	D1	$1/2\alpha$	α^2
Two-dimensional diffusion	D2	$1 - \ln(1 - \alpha)$	$[(1 - \alpha)\ln(1 - \alpha)] + \alpha$
Three-dimensional diffusion	D3	$3(1 - \alpha)^{2/3}/[2(1 - (1 - \alpha)^{1/3})]$	$[1 - (1 - \alpha)^{1/3}]^2$
Ginstling–Brounstein	D4	$3/2[(1 - \alpha)^{-1/3} - 1]$	$1 - (2\alpha/3) - (1 - \alpha)^{2/3}$
4. Sigmoid rate equations or random and subsequent growth			
Avrami–Erofeev	A2	$2(1 - \alpha)[-\ln(1 - \alpha)]^{1/2}$	$[-\ln(1 - \alpha)]^{1/2}$
Avrami–Erofeev	A3	$3(1 - \alpha)[-\ln(1 - \alpha)]^{2/3}$	$[-\ln(1 - \alpha)]^{1/3}$
Avrami–Erofeev	A4	$4(1 - \alpha)[-\ln(1 - \alpha)]^{3/4}$	$[-\ln(1 - \alpha)]^{1/4}$

Table 2 summarizes the reaction models $f(\alpha)$ and their respective integral forms $g(\alpha)$, commonly used in thermal kinetics of solid state.

Apparent activation energy calculation E_α

The activation energy E_α was evaluated by the non-isothermal isoconversional (model-free) methods using four sets of temperature. These methods are widely recommended by the International Confederation for Thermal Analysis and Calorimetry (ICTAC) [23], because they constitute accurate procedures for estimating the activation energy despite the uncertainty of the reaction mechanism, and can detect the presence of eventual complicated processes. The non-isothermal (model-free) methods are based on the isoconversional principle stating that the reaction rate depends only on temperature at constant conversion degree α , and they are able to predict the activation energy without prior knowledge about the reaction model [24]. In the present study, the activation energy calculations were achieved by the isoconversional integral methods.

From Eq. (1), the Kissinger–Akahira–Sunose (KAS) equation [25] and Flynn–Wall–Ozawa (FWO) equation [26] are deduced by a series of transforms, as can be expressed by Eqs. (2–3).

KAS equation:

$$\ln \frac{\beta}{T^2} = \ln \frac{AR}{g(\alpha)E_\alpha} - \frac{E_\alpha}{RT} \tag{2}$$

FWO equation:

$$\ln \beta = \ln \frac{0.0048AE_\alpha}{g(\alpha)R} - 1.0516 \frac{E_\alpha}{RT} \tag{3}$$

The iterative procedure [27, 28] is used to calculate the approximate E_α value approach to the exact value. The IT-KAS and IT-FWO can be expressed by Eqs. (4–5).

$$\ln \frac{\beta}{h(x)T^2} = \ln \frac{AR}{g(\alpha)E_\alpha} - \frac{E_\alpha}{RT} \tag{4}$$

$$\ln \frac{\beta}{H(x)} = \ln \frac{0.0048AE_\alpha}{g(\alpha)R} - 1.0516 \frac{E_\alpha}{RT} \tag{5}$$

where $x = E_\alpha/RT$, $h(x)$ is expressed by the fourth Senum and Yang approximation formulas [29] and $H(x)$ is also calculated from x .

$$h(x) = \frac{x^4 + 18x^3 + 86x^2 + 96x}{x^4 + 20x^3 + 120x^2 + 240x + 120} \tag{6}$$

$$H(x) = \frac{\exp(-x)h(x)/x^2}{0.0048 \exp(-1.0516x)} \tag{7}$$

The iterative procedure can be performed by using the following method [30]: we assume that $h(x) = 1$ or $H(x) = 1$, to evaluate the initial value of activation energy $E_{\alpha,1}$. The conventional isoconversional methods stop the calculation at this step. The obtained value of $E_{\alpha,1}$ is used to calculate a new value $E_{\alpha,2}$, for the activation energy from the plot of $\ln[\beta/(h(x)T^2)]$ vs. $1/T$ or $\ln[\beta/H(x)]$ vs. $1/T$ for IT-KAS and IT-FWO, respectively. This operation is repeated by replacing $E_{\alpha,1}$ with $E_{\alpha,2}$. When $|E_{\alpha,i} - E_{\alpha,i-1}| < 0.01 \text{ kJ mol}^{-1}$, the last value of $E_{\alpha,i}$ is considered to be exact value of the activation energy for the process. The estimation of the apparent activation energy by the iterative procedure does not require selection of particular kinetic model ($g(x)$ function). Therefore, the obtained E_{α} values are usually regarded as more reliable than these obtained by a single TG curve.

Determination of kinetic model

The most probable mechanism function $g(\alpha)$ of the pyrolysis reaction is deduced by rearrangement and integration of the Eq. (1):

$$g(\alpha) = \int_0^{\alpha} \frac{d\alpha}{f(\alpha)} \approx \frac{A}{\beta} \int_0^T \exp\left(\frac{-E_{\alpha}}{RT}\right) dT = \frac{AE_{\alpha}e^{-x}}{\beta R x^2} h(x) \quad (8)$$

Using Eq. (8), the experimental plot of $g(\alpha)$ versus α can be obtained. The analytical form of the reaction model can then be established by comparison between the experimental plot and the theoretical ones obtained from $g(\alpha)$ equations (Table 2), representing the reaction models, and the best matching theoretical plot can be found. The most probable mechanism function, $g(\alpha)$, of the pyrolysis reaction can also be deduced by a nonlinear model-fitting. Fitting of either single or multi-step model is commonly accomplished by means of nonlinear regression, which works by minimizing the difference between the measured and calculated data. The method of least squares (Eq. (9)) evaluates the difference in the form of the residual sum of squares (RSS) [31].

$$\text{RSS} = \sum ((y)_{\text{exp}} - (y)_{\text{calc}})^2 = \min \quad (9)$$

The pre-exponential factor A can be evaluated from the equation proposed by Malek [32]:

$$A = \frac{-\beta E_0}{RT_{\max}^2 f'(\alpha_{\max})} \exp\left(\frac{E_0}{RT_{\max}}\right) \quad (10)$$

where E_0 is the average value of E_{α} obtained by IT-KAS method. In Eq. (10), the subscript T_{\max} denotes the values

related to the maxima of the differential kinetic curves obtained at a given heating rate.

Thermodynamic parameters calculation

Some thermodynamic functions of the transition state complex (ΔS^{\ddagger} , ΔH^{\ddagger} and ΔG^{\ddagger}) of the pyrolysis reaction of oil shale may be estimated based on the following equations:

$$\Delta S^{\ddagger} = R \ln\left(\frac{Ah}{e\chi k_B T_p}\right) \quad (11)$$

$$\Delta H^{\ddagger} = E^{\ddagger} - RT_p \quad (12)$$

$$\Delta G^{\ddagger} = \Delta H^{\ddagger} - T_p \Delta S^{\ddagger} \quad (13)$$

where A is the pre-exponential factor, $e = 2.7183$ is the Neper number, χ is the transmission factor, which is unity for monomolecular reactions, k_B is the Boltzmann constant ($1.381 \cdot 10^{-23} \text{ J K}^{-1}$), h is the Plank constant ($6.626 \cdot 10^{-34} \text{ J s}$), T_p is the maximum peak temperature in DTG curves, R is the gas constant and E^{\ddagger} is the activation energy, E_0 , which can be obtained from the IT-KAS method.

Results and discussion

Mineralogical characterization

XRD analysis

The XRD patterns of the raw oil shale (ROS) and bitumen-free oil shale (FOS) treated with a conventional solvent are shown in Fig. 2. The dominant mineral phase identified in the ROS oil shale is quartz, SiO_2 (Fig. 2a). Some other minerals including clays (clinochlore, illite) and pyrite are also found in low proportions. After the separation procedure of soluble bitumen, the XRD analysis of FOS oil shale (Fig. 2b) reveals similar pattern with some differences in the diffraction peak intensity. It should be noted that the oil shale from Moroccan Rif (Arbaa Ayacha region) shows an almost absence of carbonate species as calcite or dolomite. The siliceous nature of oil shales is less frequently found, except for some world oil shales deposits such as Huadian and Indian oil shales [33, 34]. The presence of silica compound as major part may affect some characteristics of oil shales due to its adsorptive properties and thermal resistance [35]. In addition, the intensity background in

Fig. 2 XRD diagrams of ROS (a) and FOS (b) oil shales

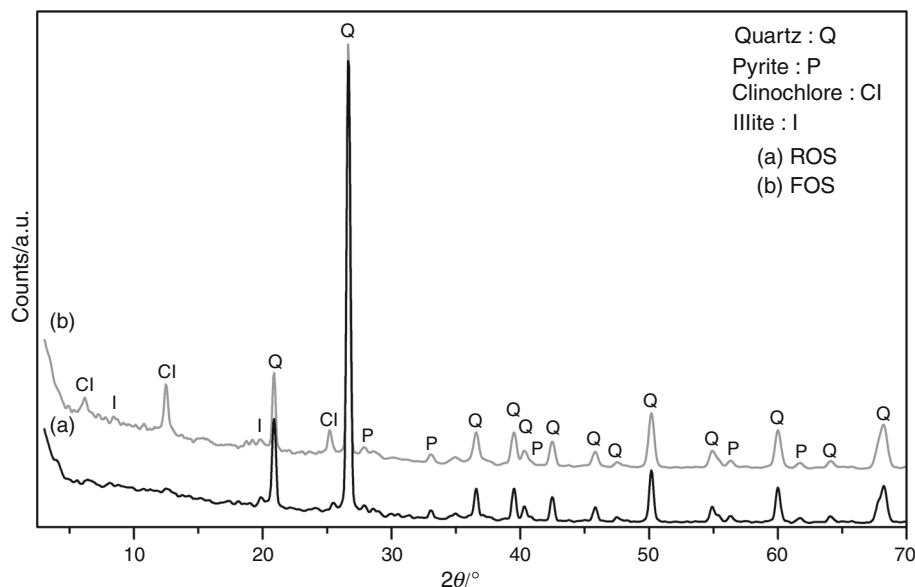


Table 3 Chemical composition of Arbaa Ayacha oil shale

(Mass%)	SiO ₂	Al ₂ O ₃	Fe ₂ O ₃	MgO	CaO	K ₂ O	Na ₂ O	TiO ₂	SO ₃	Other*	LOI
ROS	74.74	5.16	2.04	1.60	0.10	0.45	0.33	0.14	4.37	0.64	10.34
FOS	73.76	5.03	3.23	1.91	0.19	0.63	0.35	0.16	4.80	0.78	9.16

* (ZnO, MnO₂, V₂O₅, P₂O₅, Cr₂O₃, NiO, SrO, CoO)

XRD diagram of ROS sample (Fig. 2a) at lower 2θ Bragg angle was attributed to the organic material in oil shale.

XRF analysis

Table 3 shows the chemical analysis results of the raw oil shale (ROS) and bitumen-free oil shale (FOS). The proportion of major elements in the samples is expressed as the relevant oxides, in percentage. The XRF results indicate that the loss on ignition (LOI) was 10.34 and 9.16% for ROS and FOS oil shales, respectively. The loss on ignition was attributed to H₂O molecules and (OH) species issued by the decomposition of clay minerals as well as to the degradation of the disseminated organic matter. In both samples, the major oxide is silica followed by alumina and iron oxides at low percentage. The presence of Mg and Ca in small amounts illustrates the substantial absence of carbonate species, thus corroborating the XRD results. The percentage of sodium, potassium and magnesium obtained belong to the clay minerals of oil shale.

FTIR spectroscopy analysis

Figure 3 exhibits the FTIR spectra of the raw oil shale (ROS) and bitumen-free oil shale (FOS). The qualitative

interpretation of FTIR analysis results shows that the spectra consist of characteristic absorption bands of hydroxyl species and aliphatics and aromatics of organic matter of oil shales which partially overlapped with bands associated to mineral matrix. The mineral part displays intense bands between 1200–900 and 850–400 cm⁻¹, attributed to clay silicates and quartz, in the both studied samples. In these absorption regions, the presence of pyrite is not excluded as shown in several IR studies of oil shales [36, 37]. The broadband ranged between 3700 and 3200 cm⁻¹ belongs to H₂O and OH of mineral matrix and OH of organic groups (alcohol, phenol and carboxyl). The presence of organic matter is illustrated in 3200–2700 cm⁻¹ and 1500–1380 cm⁻¹ regions, by absorption bands C–H of aliphatics (CH₂ and CH₃) [38, 39]. These bands are visible in the ROS oil shale (Fig. 3a), while they diminish in intensity in the spectrum of FOS oil shale (Fig. 3b), justifying the removal of soluble bitumen in FOS oil shale by the conventional solvents. The appearance of these bands at low intensities (Fig. 3b) is due essentially to C–H species of insoluble kerogen matter. The bands observed in the range 1800–1600 cm⁻¹ are assigned to elongation vibrations of double bonds carbon–carbon of aromatics and olefin species and also of carbonyl functions present in the kerogen macrostructure [40].

Fig. 3 IRTF spectra of ROS (a) and FOS (b) oil shales

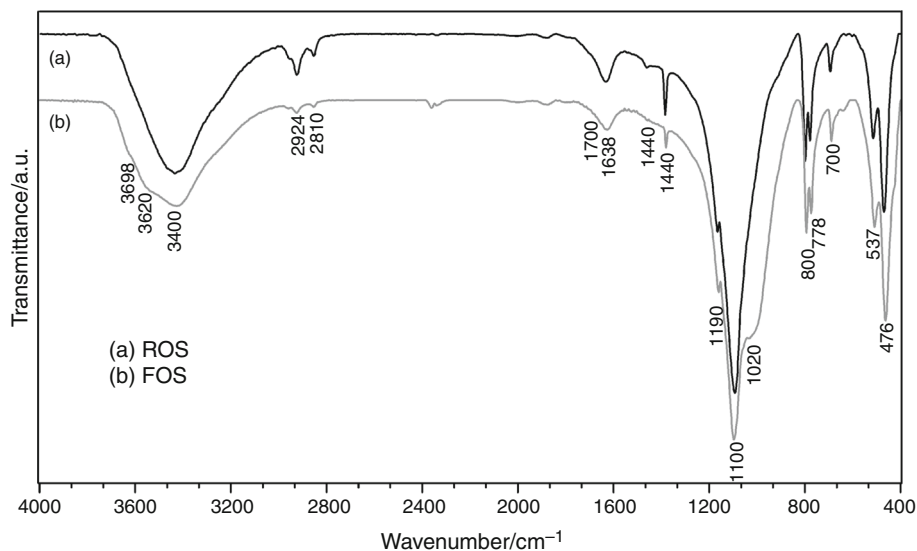
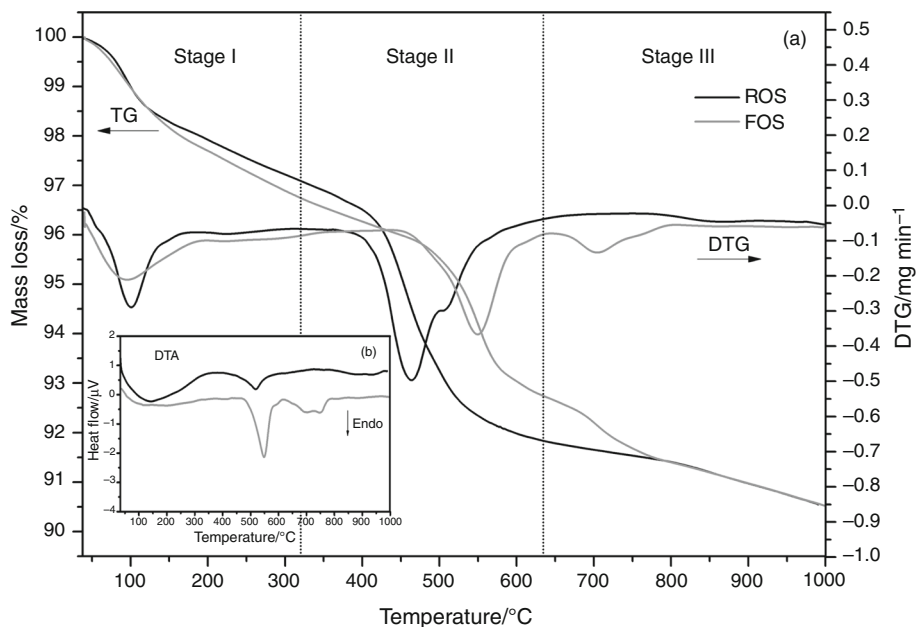


Fig. 4 TG/DTG (a) DTA (b) curves of ROS and FOS oil shales



Thermal analysis

The non-isothermal pyrolysis of the raw oil shale (ROS) and bitumen-free oil shale (FOS) was carried out at $10\text{ }^\circ\text{C min}^{-1}$ under flowing nitrogen atmosphere (60 mL min^{-1}) and initial mass of $10.0 \pm 0.1\text{ mg}$, from ambient temperature up to $1000\text{ }^\circ\text{C}$. The typical TG, DTG and DTA curves are presented in Fig. 4. As the two samples display similar pyrolysis characteristics, both the mass loss processes can be divided into three stages (Fig. 4a). The similar thermal behavior is also observed in many reported thermal studies of oil shales [41, 42]. In the first stage ($<325\text{ }^\circ\text{C}$), the mass loss is mainly attributed to evaporation of moisture, interlayer water from clay

minerals and to water of OH condensation, which accounts for almost 3% of the initial mass. In the second stage ($325\text{--}630\text{ }^\circ\text{C}$), the observed mass losses, 6% for ROS and $\sim 4\%$ for FOS oil shale, corresponding to maximum DTG curves at 460 and $540\text{ }^\circ\text{C}$, respectively, are assigned to endothermic decomposition of organic matter (Fig. 4b), including bitumen and kerogen for the first sample and only kerogen for the second. According to literature data, this stage is considered as the oil shale producing stage in oil shale pyrolysis [11]. It should be emphasized that the pyrolysis of kerogen in samples is shifted toward high temperatures by comparison with other oil shales containing carbonates. This is certainly due to the inhibitive effect of the mineral matrix which consists primarily of silica as

was observed in pyrolysis study of Turkish Göynük and US Green River oil shales [43, 44]. As we aforementioned, the mineral silica matrix has a high adsorption capacity and thermal resistance toward the organic matter, thus delaying the pyrolysis process in this temperature region. Similar behavior was also observed in other siliceous oil shales [37]. In the third stage (>630 °C), the final mass loss for ROS oil shale ($<1\%$), which is represented by a deflection of the base line, is governed by the thermal decomposition of inorganic minerals such as clay minerals and pyrite [20]. The absence of the decomposition reaction of carbonate species, which normally occurs at about 800 °C, confirms our above results. For FOS oil shale, the mass loss ($\sim 2\%$) corresponding to maximum DTG curve at 695 °C is dominated by an endothermic effect. This endothermic effect (Fig. 4b), called Boudouard reaction, may occur when CO_2 released during the pyrolysis from organic matter and reacts with char to produce CO. This reaction is favored by high temperature and low pressure [45, 46]. The high temperature also promotes the decomposition of pyrite that one cannot exclude [46, 47].

Kinetic study

The kinetic measurements of ROS and FOS oil shales were conducted under pure nitrogen atmosphere using the non-isothermal methods and four sets of heating rates (5, 10, 15 and 20 °C min^{-1}), at temperature range 30–1000 °C. According to American ASTM standard (E11) and ICTAC recommendations, the samples were crushed and sieved to less than 80 meshes in the average particle diameter to reduce the effects of heat and mass transfers during pyrolysis. The kinetic study was limited to stage II as shown in Fig. 4, since it represents the main pyrolysis processing of the organic matter into hydrocarbons. For

comparison purposes, we considered here only the process corresponding to kerogen pyrolysis of ROS oil shale, after performing deconvolution procedure. More details are described in our previous article [1]. Then, the thermal behaviors of kerogen-ROS and FOS oil shales, represented by $[(d\alpha/dt) - T]$ curves are illustrated in Fig. 5.

Thermal kinetics of kerogen-ROS and FOS oil shales, characterized by the curves $[d\alpha/dt - T]$ show that the maximum rates ($d\alpha/dt$) shift systematically toward higher temperatures when the heating rate increases. Such behavior was observed in almost all the world's oil shales. This is due to the temperature gradient inside and outside the particles, which is lower at lower heating rates and longer is the exposure of sample to a particular temperature [48, 49]. As can be seen in Fig. 5, the variation of the heating rate did not alter the kinetic curves and consequently the kinetic parameters should not be changed.

Determination of activation energy by model-free method

The isoconversional methods of KAS, FWO and their corresponding IT-KAS and IT-FWO were used to calculate the distribution of activation energy curves ($E_\alpha - \alpha$) at the major oil-producing stage (Stage II) (Fig. 4), precisely the peak observed in thermal curves related to the kerogen decomposition, for both samples.

Figure 6a–d displays the variation of $(E_\alpha - \alpha)$, for kerogen-ROS and FOS oil shales. The average values of E_α , illustrated in Table 4, can be estimated in the range of α between [0.2 and 0.8].

As can be seen from Fig. 6, the distribution of E_α versus α , for kerogen-ROS and FOS oil shales, presents the same trend in the range of [0.2–0.8] and appears for each method to be approximately constant with respect to the conversion rate α . According to several decomposition kinetics, if the

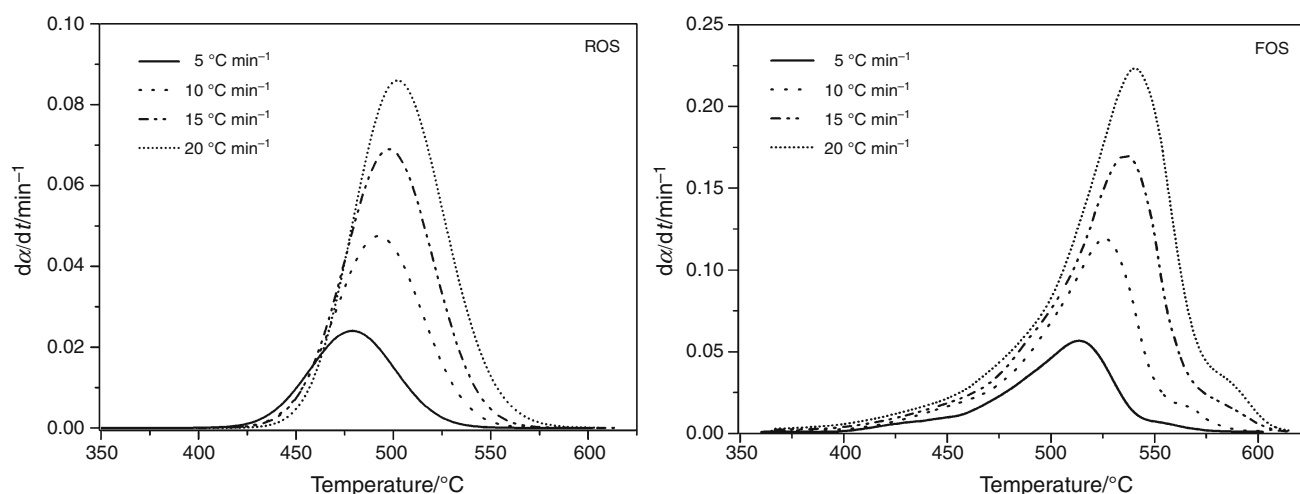


Fig. 5 Thermal curves $[d\alpha/dt - T]$ of Kerogen-ROS and FOS oil shales at different heating rates

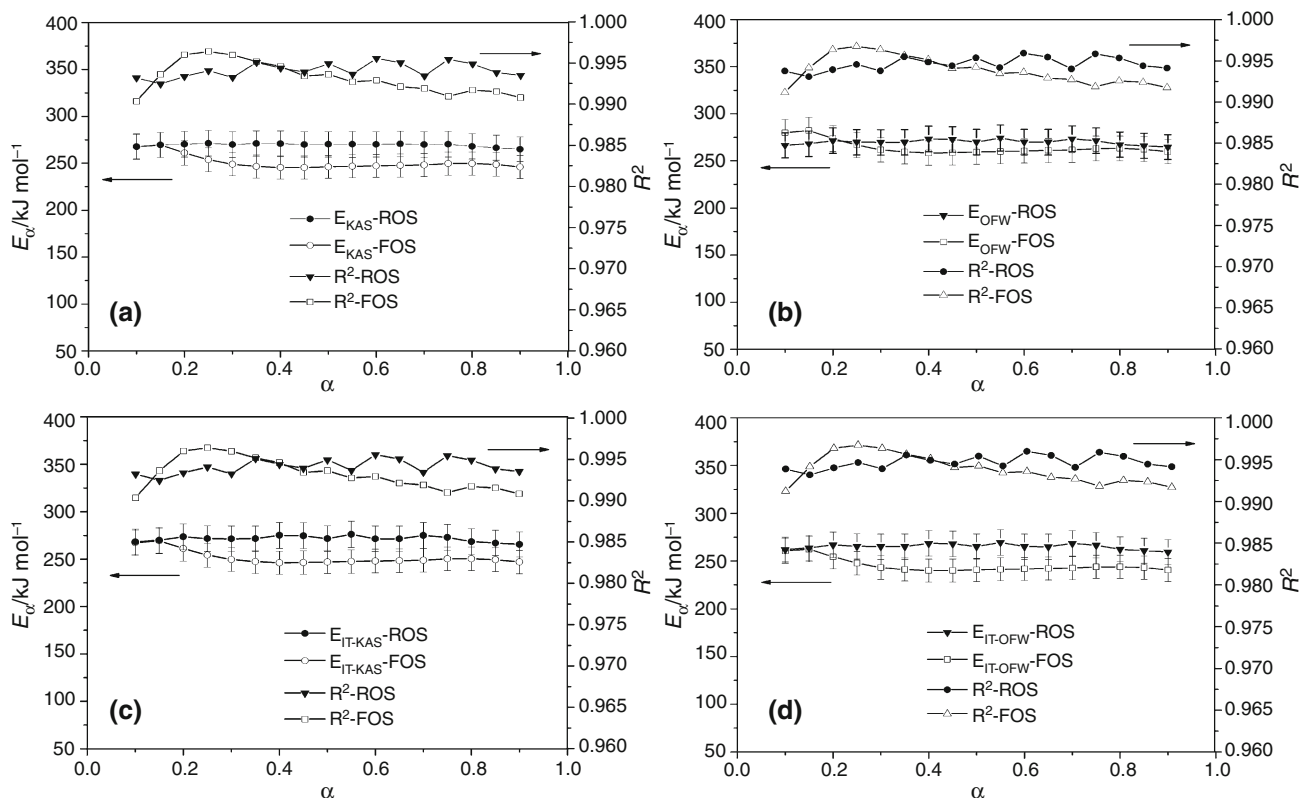


Fig. 6 ($E_\alpha - \alpha$) curves of Kerogen-ROS and FOS oil shales calculated by KAS, OFW and IT-KAS and IT-OFW methods

Table 4 Average values E_α for Kerogen-ROS and FOS oil shales

Oil shales	$E_{KAS}/\text{kJ mol}^{-1}$	SD	$E_{IT-KAS}/\text{kJ mol}^{-1}$	SD	$E_{OFW}/\text{kJ mol}^{-1}$	SD	$E_{IT-OFW}/\text{kJ mol}^{-1}$	SD
Kerogen-ROS	270.23	2.00	272.72	2.11	269.15	1.88	266.16	1.96
FOS	248.92	4.28	249.24	4.34	262.12	4.15	249.62	4.06

standard deviation SD of E_α is lower than 10%, the decomposition process is dominated by a single reaction step; otherwise, it should be interpreted in terms of a multi-step mechanism [50, 51]. Figure 6 shows that E_α values are almost independent of α with SD do not exceed 4.5% (Table 4). So, this indicates that the thermal decomposition of both samples can be considered as a single-step reaction mechanism and described by a simple kinetic triplet [E_α , $g(\alpha)$ and A]. The average value, E_α , calculated by KAS and FWO methods is very close to values from their corresponding IT-KAS and IT-FWO methods (Table 4). The average E_α values, for kerogen-ROS and FOS oil shales, are larger than what is reported in numerous oil shales, but consistent with our recent experimental energy results gained in pyrolysis of original Moroccan Rif oil shale (Arbaa Ayacha region) [1] and energy values found in Brazilian and Chinese oil shales [11, 52, 53]. The high values of energy depend on the type and composition of

kerogen, but also on the nature of the host mineral matrix which consists mainly of silica or carbonates. The presence of silica in oil shale as a major compound has an inhibiting effect due to its high adsorptive properties and refractory, as mentioned above. Similar findings have also been reported in studying the pyrolysis of Turkish and US Green River oil shales [43].

Determination of the most probable kinetic model

The determination of reaction model can be accomplished by using Eq. (8), to generate experimental plots of $g(\alpha)$ versus α . Figure 7 displays the experimental curve ($\beta = 10 \text{ }^\circ\text{C min}^{-1}$) and theoretical $g(\alpha)$ for various models which present an excellent value of regression coefficient R^2 close to 1.

The resulting experimental plots ($\beta = 10 \text{ }^\circ\text{C min}^{-1}$) do not show any significant deviation with other used heating

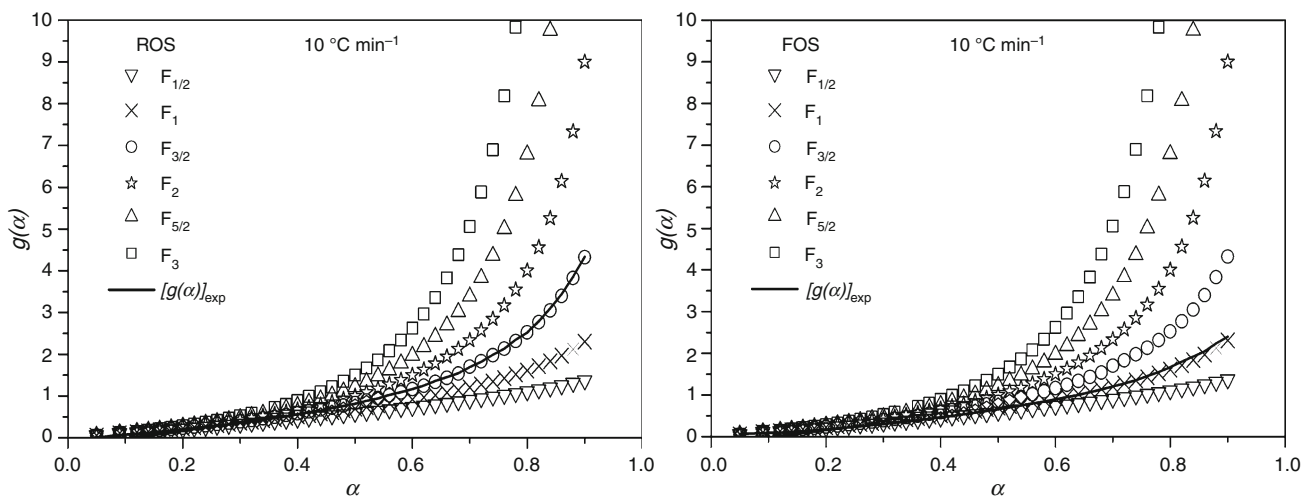


Fig. 7 Comparison between theoretical models (different symbols) and experimental results, for $\beta = 10 \text{ }^\circ\text{C min}^{-1}$ (dark solid line)

Table 5 Kinetic parameters of Kerogen-ROS and FOS oil shales

Oil shales	Kerogen-ROS			FOS		
	n	$\ln A$	RSS	n	$\ln A$	RSS
$\beta/^\circ\text{C min}^{-1}$						
5	1.556	42.31	0.0590	1.072	36.72	0.1829
10	1.535	42.25	0.0953	1.074	36.82	0.1782
15	1.532	42.33	0.0531	1.068	36.24	0.1855
20	1.579	42.28	0.0262	1.070	36.74	0.1967
Average	1.550	42.30		1.071	36.63	

rates. From the comparison of theoretical models curves and experimental plot at $\beta = 10 \text{ }^\circ\text{C min}^{-1}$ and by using the IT-KAS average value of E_α (Fig. 7), the most probable mechanism functions for both samples are roughly determined and correspond to the reaction order model, F_n , with $n = 3/2$, for kerogen-ROS, and $n = 1$, for FOS oil shales. The kinetic parameters of kerogen pyrolysis appear to be simplified slightly by removing bitumen from ROS oil shale. Thus, the kinetic pyrolysis of Moroccan kerogen-ROS and FOS oil shales lead to the integral forms of $g(\alpha)$ mechanism as follows:

For kerogen - ROS oil shale : $F_{3/2}$;

$$g(\alpha) = 2 \left[(1 - \alpha)^{1/2} - 1 \right] \tag{14}$$

For FOS oil shale : F_1 ; $g(\alpha) = -\ln(1 - \alpha)$ (15)

Using the nonlinear regression procedure for refinement of the kinetic parameters, the exact value of “ n ” giving the best fit can be obtained from the general integral form (Eq. (16)) by minimizing the RSS factor (Eq. (9)), for every heating rate. The obtained results are summarized in Table 5.

$$g(\alpha) = \left[1 - (1 - \alpha)^{1-n} \right] / (1 - n) \tag{16}$$

The determination of pre-exponential factor, for the pyrolysis reaction of kerogen-ROS and FOS oil shales, was estimated by using Eqs. (9–10). The obtained results are very close to $\ln A$ values calculated from KAS and FWO methods, thereby confirming the proposed kinetic model F_n (chemical reaction model). In solid-state reactions, low pre-exponential factors will often indicate a surface reaction or demonstrate the presence of “tight” complex. High factors (A) will usually indicate a “loose” complex. Even higher factors can be obtained for complexes having free translation on the surface [54, 55]. Based on these considerations, the pre-exponential factor calculated for kerogen-ROS oil shale is $A = 2.35 \cdot 10^{18} \text{ min}^{-1}$ and for FOS oil shale is $A = 8.10 \cdot 10^{15} \text{ min}^{-1}$. These values indicate that pyrolysis is “loose” complex process, for both samples.

From all results, the kinetic equations for the pyrolysis of kerogen-ROS and FOS oil shales, under non-isothermal conditions, can be written as follows, Eqs. (17, 18):

Kerogen - ROS oil shale :

$$\left(\frac{d\alpha}{dt} \right)_{\text{Kerogen-ROS}} = 2.35 \cdot 10^{18} e^{-272.72/RT} (1 - \alpha)^{1.550} \tag{17}$$

FOS oil shale :

$$\left(\frac{d\alpha}{dt} \right)_{\text{FOS}} = 8.10 \cdot 10^{15} e^{-249.24/RT} (1 - \alpha^{1.071}) \tag{18}$$

Table 6 Thermodynamic parameters of Kerogen-ROS and FOS oil shales

Oil shales	$\Delta S^\ddagger /$ $\text{J mol}^{-1} \text{ K}^{-1}$	$\Delta H^\ddagger /$ kJ mol^{-1}	$\Delta G^\ddagger /$ kJ mol^{-1}
Kerogen-ROS	90.55	266.35	196.96
FOS	43.09	242.57	208.02

Based on these results, it seems that the presence or not of bitumen did not affect the pyrolysis mechanism of oil shale especially for kerogen, except the reaction order which has been changed. Therefore, the mechanisms governing the pyrolysis reaction of kerogen and bitumen in Moroccan Rif oil shale are independent, as has been indicated in our previous work [1] and in some literature data [56, 57].

Determination of thermodynamic parameters

Equations (11–13) were used to estimate the thermodynamic functions of the transition state complex (ΔS^\ddagger , ΔH^\ddagger and ΔG^\ddagger), for kerogen-ROS and FOS oil shales at all heating rates. The average values of the thermodynamic parameters are summarized in Table 6.

As can be seen from Table 6, the positive values of activation entropy ΔS^\ddagger , for both samples, indicate the presence of malleable-activated complexes, which lead to a large number of freedom degrees for rotation and vibration [58]. The positive ΔH^\ddagger values agree with the endothermic effect recorded during oil shale pyrolysis. The positive values of the free Gibbs energy ΔG^\ddagger show that the pyrolysis of kerogen-ROS and FOS oil shales is non-spontaneous reaction and needs heat to occur, under atmosphere pressure. These results are in accordance with thermal analysis data.

Conclusions

In this research, the mineralogical characterization of raw oil shale (ROS) and bitumen-free oil shale (FOS) from Moroccan Rif region was studied. The mineral part of oil shales is found predominantly siliceous illustrated by high content of silica. The study also includes a contribution to understanding the effect of soluble bitumen on the thermal degradation of kerogen contained in oil shales studied. Thus, the pyrolysis reaction kinetics of kerogen-ROS and FOS oil shales have been estimated and compared by using non-isothermal isoconversional and nonlinear model-fitting methods. For both samples, the curves of activation energy versus α indicate that pyrolysis proceeds in single-step kinetic process, which can be described by a unique kinetic triplet [E_a , A , $g(\alpha)$]. The most probable mechanism for the pyrolysis stage was adequately evaluated by reaction order equation (chemical reaction), with F3/2 and F1 models for kerogen-ROS and FOS oil shales, respectively. The removal of bitumen from oil shales did not seem to modify the reaction mechanism but only affects the order of the reaction. The pyrolysis of bitumen and kerogen in oil shales are practically independent reactions, and no relation was observed in thermal kinetics calculations between soluble bitumen and kerogen-oil shales.

Acknowledgements This research was financially supported by University of Mohammed V-Morocco under the Project No. SCH 04/09 and Hassan II Academy of Science and Technology, Morocco.

References

- Moine EC, Groune K, El Hamidi A, Khachani M, Halim M, Arsalane S. Multistep process kinetics of the non-isothermal pyrolysis of Moroccan Rif oil shale. *Energy*. 2016;115:931–41.
- Külaots I, Goldfarb JL, Suuberg EM. Characterization of Chinese, American and Estonian oil shale semicokes and their sorptive potential. *Fuel*. 2010;89(11):3300–6.
- Li SY, Yue CT. Study of pyrolysis kinetics of oil shale. *Fuel*. 2003;82(3):337–42.
- Kök MV, Pamir MR. ASTM kinetics of oil shales. *J Therm Anal Calorim*. 1998;53(2):567–75.
- Ballice L. Stepwise chemical demineralization of Göynük (Turkey) oil shale and pyrolysis of demineralization products. *Ind Eng Chem Res*. 2006;45(3):906–12.
- Muhammad AF, El Salmawy MS, Abdalaala AM, Sameah S, El-Nakhil oil shale: material characterization and effect of acid leaching. *Oil Shale*. 2011;28(4):528–47.
- Thakur DS, Nuttall HE. Kinetics of pyrolysis of Moroccan oil shale by thermogravimetry. *Ind Eng Chem Res*. 1987;26(7):1351–6.
- Bar H, Ikan R, Aizenshtat Z. Comparative study of the isothermal pyrolysis kinetic behaviour of some oil shales and coals. *J Anal Appl Pyrol*. 1988;14(1):49–71.
- Dogan OM, Uysal BZ. Non-isothermal pyrolysis kinetics of three Turkish oil shales. *Fuel*. 1996;75(12):1424–8.
- Torrente MC, Galan MA. Kinetics of the thermal decomposition of oil shale from Puertollano (Spain). *Fuel*. 2001;80(3):327–34.
- Bai FT, Wei G, Lü XS, Liu YM, Guo MY, Li Q, Sun Y. Kinetic study on the pyrolysis behavior of Huadian oil shale via non-isothermal thermogravimetric data. *Fuel*. 2015;146:111–8.
- Rajeshwar K. The kinetics of the thermal decomposition of green river oil shale kerogen by non-isothermal thermogravimetry. *Thermochim Acta*. 1981;45(3):253–63.
- Kök MV, Senguler I, Hufnagel H, Sonel N. Thermal and geochemical investigation of Seyitomer oil shale. *Thermochim Acta*. 2001;371(1–2):111–9.
- Kök MV. Thermal investigation of Seyitomer oil shale. *Thermochim Acta*. 2001;369(1–2):149–55.
- Perejón A, Sánchez-Jiménez PE, Criado JM, Pérez-Maqueda LA. Kinetic analysis of complex solid-state reactions. A new deconvolution procedure. *J Phys Chem B*. 2011;115(8):1780–91.
- Koga N, Goshi Y, Yamada S, Pérez-Maqueda LA. Kinetic approach to partially overlapped thermal decomposition processes. *J Therm Anal Calorim*. 2013;111(2):1463–74.
- Liu QQ, Hang XX, Li QY, Huang YR, Jiang XM. TG-DSC analysis of pyrolysis process of two Chinese oil shales. *J Therm Anal Calorim*. 2014;116(1):511–7.
- Wang W, Li S, Yue C, Ma Y. Multistep pyrolysis kinetics of North Korean oil shale. *J Therm Anal Calorim*. 2015;119(1):643–9.
- Moine EC, Tangarfa M, Khachani M, El Hamidi A, Halim M, Arsalane S. Thermal oxidation study of Moroccan oil shale: a new approach to non-isothermal kinetics based on deconvolution procedure. *Fuel*. 2016;180:529–37.
- Groune K, Halim M, Benmakhlof M, Arsalane S, Lemee L, Ambles A. Organic geochemical and mineralogical characterization of the Moroccan Rif bituminous rocks. *J Mater Environ Sci*. 2013;4(4):472–81.

21. Groune K, Halim M, Arsalane S. Thermal and mineralogical studies of Moroccan Rif bituminous rocks. *Oil Shale*. 2013;30(4):536–49.
22. Vyazovkin S, Chrissafis K, Di Lorenzo ML, Koga N, Pijolat M, Roduit B, Sbirrazzuoli N, Suñol JJ. ICTAC kinetics committee recommendations for collecting experimental thermal analysis data for kinetic computations. *Thermochim Acta*. 2014;590:1–23.
23. Vyazovkin S, Burnham AK, Criado JM, Pérez-Maqueda LA, Popescu C, Sbirrazzuoli N. ICTAC kinetics committee recommendations for performing kinetic computations on thermal analysis data. *Thermochim Acta*. 2011;520(1–2):1–19.
24. Brown ME, Maciejewski M, Vyazovkin S, Nomen R, Sempere J, Burnham A, Opfermann J, Strey R, Anderson HL, Kemmler A, Keuleers R, Janssens J, Desseyn HO, Li CR, Tang TB, Roduit B, Malek J, Mitsunashi T. Computational aspects of kinetic analysis. Part A: the ICTAC kinetics project-data, methods and results. *Thermochim Acta*. 2000;355(1–2):125–43.
25. Akahira T, Sunose T. Method of determining activation deterioration constant of electrical insulating materials. *Res Rep Chiba Inst Technol (Sci Technol)*. 1971;16:22–31.
26. Flynn JH. The isoconversional method for determination of energy of activation at constant heating rates, corrections for the Doyle approximation. *J Therm Anal Calorim*. 1983;27(1):95–102.
27. Chunxiu G, Yufang S, Donghua C. Comparative method to evaluate reliable kinetic triplets of thermal decomposition reactions. *J Therm Anal Calorim*. 2004;76(1):203–16.
28. Su TT, Jiang H, Gong H. Thermal stabilities and the thermal degradation kinetics of poly(ϵ -Caprolactone). *Polym Plast Technol Eng*. 2008;47(4):398–403.
29. Senum GI, Yang RT. Rational approximations of the integral of the Arrhenius function. *J Therm Anal Calorim*. 1977;11(3):445–7.
30. Chen ZP, Chai Q, Liao S, He Y, Li Y, Bo XH, Wu WW, Li B. Application of isoconversional calculation procedure to non-isothermal kinetic study: III. Thermal decomposition of ammonium cobalt phosphate hydrate. *Thermochim Acta*. 2012;543:205–10.
31. Slovák V. Determination of kinetic parameters by direct non-linear regression from TG curves. *Thermochim Acta*. 2001;372(1–2):175–82.
32. Málek J. A computer program for kinetic analysis of non-isothermal thermoanalytical data. *Thermochim Acta*. 1989;138(2):337–46.
33. Wang Z, Deng S, Gu Q, Zhang Y, Cui X, Wang H. Pyrolysis kinetic study of Huadian oil shale, spent oil shale and their mixtures by thermogravimetric analysis. *Fuel Process Technol*. 2013;110:103–8.
34. Kumar R, Bansal V, Badhe RM, Madhira ISS, Sugumaran V, Ahmed S, Christopher J, Patel MB, Basu B. Characterization of Indian origin oil shale using advanced analytical techniques. *Fuel*. 2013;113:610–6.
35. Patterson JH. A review of the effects of minerals in processing of Australian oils shales. *Fuel*. 1994;73(3):321–7.
36. Adams MJ, Awaja F, Bhargava S, Grocott S, Romeo M. Prediction of oil yield from oil shale minerals using diffuse reflectance infrared Fourier transform spectroscopy. *Fuel*. 2005;84(14–15):1986–91.
37. Sun YH, Bai FT, Liu BC, Liu YM, Guo MY, Guo W, Wang QW, Lü XS, Yang F, Yang Y. Characterization of the oil shale products derived via topochemical reaction method. *Fuel*. 2014;115:338–46.
38. Bruan V, Halim M, Ziyad M, Largeau M, Ambles A. Characterization of the Moroccan Timahdit (X-layer) oil shale kerogen using pyrolysis and thermally assisted hydrolysis and methylation. *J Anal Appl Pyrol*. 2001;61(1–2):165–79.
39. Aboulkas A, El Harfi K. Effects of acid treatments on Moroccan Tarfaya oil shale and pyrolysis of oil shale and their kerogen. *J Fuel Chem Technol*. 2009;37(6):659–67.
40. Ambles A, Halim M, Jacquesy JC, Vitorovic D, Ziyad M. Characterization of kerogen from Timahdit shale (Y-layer) based on multistage alkaline permanganate degradation. *Fuel*. 1994;73(1):17–24.
41. Kaljuvee T, Keelmann M, Trikkel A, Kuusik R. Thermooxidative decomposition of oil shales. *J Therm Anal Calorim*. 2011;105(2):395–403.
42. Sun YH, Bai FT, Lü XS, Jia CX, Wang Q, Guo MY, et al. Kinetic study of Huadian oil shale combustion using a multi-stage parallel reaction model. *Energy*. 2015;82:705–13.
43. Karabakan A, Yürüm Y. Effect of the mineral matrix in the reactions of oil shales: 1. Pyrolysis reactions of Turkish Göynük and US Green River oil shales. *Fuel*. 1998;77(12):1303–9.
44. Sert M, Ballice L, Yüksel M, Sağlam M. The effect of acid treatment on the pyrolysis of Göynük oil shale (Turkey) by thermogravimetric analysis. *Oil Shale*. 2012;29(1):51–62.
45. Shabbar S, Rana Q, Ilham T, Isam J. Kinetics of pyrolysis and combustion of oil shale sample from thermogravimetric data. *Fuel*. 2011;90(4):1631–7.
46. Yan JW, Jiang XM, Han XX, Liu JG. A TG–FTIR investigation to the catalytic effect of mineral matrix in oil shale on the pyrolysis and combustion of kerogen. *Fuel*. 2013;104:307–17.
47. Hu G, Dam-Johansen K, Wedel S, Hansen JP. Decomposition and oxidation of pyrite. *Prog Energy Combust Sci*. 2006;32(3):295–314.
48. Gil MV, Casal D, Pevida C, Pis JJ, Rubiera F. Thermal behaviour and kinetics of coal/biomass blends during co-combustion. *Bioresour Technol*. 2010;101(14):5601–8.
49. Bai FT, Sun YH, Liu YM, Li Q, Guo MY. Thermal and kinetic characteristics of pyrolysis and combustion of three oil shales. *Energy Convers Manag*. 2015;97:374–81.
50. Xia Y, Huang Y, Li Y, Liao S, Long Q, Liang J. LiPO₄: Ce, Tb, Yb Phosphor-synthesis and kinetics study for thermal process of precursor by Vyazovkin, OFW, KAS, Staring, and Mastplots methods. *J Therm Anal Calorim*. 2015;120(3):1635–43.
51. Shahcheraghi SH, Khayati GR. Kinetics analysis of the non-isothermal decomposition of Ag₂O–graphite mixture. *J Trans Nonferrous Met Soc China*. 2014;24(9):2991–3000.
52. Jankovic B. The kinetic modeling of the non-isothermal pyrolysis of Brazilian oil shale: application of the Weibull probability mixture model. *J Pet Sci Eng*. 2013;11:25–36.
53. Cordes HM. Pre-exponential factors for solid-state thermal decomposition. *J Phys Chem*. 1968;72(6):2185–9.
54. Wang Q, Liu HP, Sun BZ, Li SH. Study on pyrolysis characteristics of Huadian oil shale with isoconversional method. *Oil Shale*. 2009;26(2):148–62.
55. Chen Z, Chai Q, Liao S, Chen X, He Y, Li Y, Wu W, Li B. Nonisothermal kinetic study: IV. Comparative methods to evaluate E_{α} for thermal decomposition of KZn₂(PO₄)(HPO₄) synthesized by a simple route. *Ind Eng Chem Res*. 2012;515(26):8985–91.
56. Tiwari P, Deo M. Detailed kinetic analysis of oil shale pyrolysis TGA data. *AIChE J*. 2012;58(2):505–15.
57. Wang W, Li SY, Li LY, Ma Y, Yue CT, He JL. Pyrolysis kinetic of North-Korean oil shale. *Oil Shale*. 2014;31(3):250–65.
58. Boonchom B. Kinetic and thermodynamic studies of MgHPO₄·3H₂O by non-isothermal decomposition data. *J Therm Anal Calorim*. 2009;98(3):863–71.